AIP | Journal of Applied Physics

Analysis of plasma-modes of a gated bilayer system in high electron mobility transistors

Shubhendu Bhardwaj, Siddharth Rajan, and John L. Volakis

Citation: Journal of Applied Physics **119**, 193102 (2016); doi: 10.1063/1.4950795
View online: http://dx.doi.org/10.1063/1.4950795
View Table of Contents: http://scitation.aip.org/content/aip/journal/jap/119/19?ver=pdfcov
Published by the AIP Publishing

Analysis of plasma-modes of a gated bilayer system in high electron mobility transistors

Shubhendu Bhardwaj, Siddharth Rajan, and John L. Volakis
Department of Electrical and Computer Engineering, The Ohio State University, Columbus, Ohio 43212, USA

(Received 16 March 2016; accepted 5 May 2016; published online 17 May 2016)

We present rigorous analytical and computational models to study the plasma-waves in a gated-bilayer system present in a double-channel high electron mobility transistor. By analytically deriving the dispersion relations, we have identified the optical and acoustic modes in such systems. We find that the presence of the metal gate selectively modifies the optical plasmons of an ungated-bilayer, while the acoustic plasmons remain largely unchanged. Analysis shows that these modified optical plasmons could be advantageous for resonant and non-resonant plasma-wave devices. The paper further serves to verify our analytical formulae using a full-wave hydrodynamic numerical solver, based on finite difference time domain algorithm. Using the solver, we examine these modes in the gated/ungated bilayers under a plane wave excitation. We observe that, most incident power couples to the optical mode for such an excitation. Nevertheless, acoustic modes can also be excited, if the discontinuity dimensions are optimized accordingly. These observations are also explained using 2D field-plots for the first time, thus providing intuitive understanding of the plasmon excitation in the bilayers. *Published by AIP Publishing.* [http://dx.doi.org/10.1063/1.4950795]

I. INTRODUCTION

Plasma-wave electronics are of interest due to their potential for terahertz devices. Indeed, the terahertz emitters and detector configurations that rely on plasma-wave oscillations have been proposed in the past.[1–6] It is therefore important to understand the properties of these plasma-waves via analytical means. For single channel systems, this analytical work can be referred from the prior work.[7–12] In this paper, we are concerned with double channel high electron mobility transistors (HEMTs), i.e., HEMT devices containing closely placed 2DEG channels in a gated configuration[13,14] (see Fig. 1). Such double (or multiple) channel HEMTs lead to increased electron densities for improving the overall channel conductivity. As a result, these provide a new approach for designing of modern terahertz emitters and detectors.

The theoretical analysis of the plasma-waves in such two channel systems (also known as bilayer) has been considered previously.[15,16] These showed that small inter-channel distances ($\Delta d \ll \lambda_p$, λ_p being plasmon wavelength) imply a strong electromagnetic coupling that leads to collective plasmonic modes in the channels. Two such modes have been identified: (1) optical mode, caused due to in-phase oscillations of the electron densities in the two channels; and (2) acoustic mode, arising due to out-of-phase oscillations. These modes have also been confirmed experimentally as demonstrated in Ref. 17, among others. Inter-channel tunneling is also possible in a bilayer configuration leading to interesting physics in such systems, as theoretically and experimentally demonstrated in Refs. 18 and 19.

In the theoretical work so far, the bilayer structure was placed in an ungated environment, i.e., the bilayer is assumed to be embedded in homogeneous or heterogeneous dielectric media. In this paper, we instead consider a practically relevant case. Specifically, the bilayer or the dual channel is placed in the vicinity of the metal gate. Such metal gates are frequently used to provide free-space coupling of plasmons and for modulating the electron density.[20–22] Recently, a gate was shown to modulate electron densities in multiple overlaying channels using a castellated configuration.[23] Another practical scenario of the gated bilayer is tunneling coupled bilayer where the gate voltage is used to tune the subband energy levels.[19] We note that prior to this work, gate considerations were also made for the double gated graphene bilayers in Ref. 24, but dispersion relations have yet to be derived.

In this work, we will derive dispersion relations for the gated double channels or bilayers using electromagnetic field profiles between the channels (similar to Ref. 8). We find that the presence of the metal-gate can selectively affect the optical plasmonic modes in the bilayer. This implies a decrease in their wavelength and thus an increase in the attenuation constant (Np/μm). However, the acoustic plasmons remain unchanged in the presence of the metal gate. These observations are then verified using our full-wave-hydrodynamic finite difference time domain (FDTD) solver. The solver is subsequently used to examine these modes in the gated/ungated bilayers. Specifically, we study the

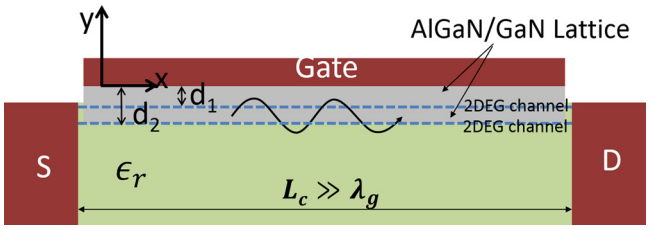

FIG. 1. Schematic of the double channel HEMT device based on the GaN/AlGaN lattice.

mechanism of coupling of these modes, excited by an incident plane wave.

II. DISPERSION OF PLASMA-WAVES IN A GATED DOUBLE CHANNEL 2DEG: SMALL SIGNAL ANALYSIS

We consider a long, thin 2DEG channel placed under a metallic gate at a vertical distance d_1 (see Fig. 1). A second 2DEG channel is positioned at a distance d_2 from the metallic gate. We also assume a drain-to-source bias to enable drift velocities v_{o1} and v_{o2} in the upper and lower channels, respectively. The corresponding initial electron densities in the two channels are assumed to be n_{o1} and n_{o2}, respectively. To calculate the dispersion relation, we proceed to first calculate the AC conductivity of the channel using hydrodynamic equations. Next, we solve for the EM-fields within the channel and in its vicinity, subject to the boundary conditions in the 2DEG and gate. The derived EM-fields are then used to produce the dispersion relation.

Below, we consider the currents and fields in the upper channel to calculate its AC conductivity. To begin with, we invoke the hydrodynamic approximations based on Boltzmann's Transport Equations (BTE).[25] That is, we consider continuity equation coupled with the momentum conservation equations, viz.,

$$\frac{\partial n_1}{\partial t}+\frac{\partial j_1}{\partial x}=0, \tag{1}$$

$$\frac{\partial j_1}{\partial t}+v_1\frac{\partial j_1}{\partial x}+j_1\frac{\partial v_1}{\partial x}=-\frac{qn_1E_{x1}}{m_e}-\frac{j_1}{\tau}, \tag{2}$$

where $j_1(=n_1v_1)$ is the sheet electron flux with n_1 and v_1 being the total electron density (i.e., AC and DC) and velocity in the 2DEG channel. E_{x1} is the x-directed electric field along the channel. In addition, τ refers to the momentum relaxation time, and m_e is the effective electron mass and $q=1.6\times10^{-19}$ C is the charge on a single electron.

For small signal analysis, we assume that an electric field of the form $E_{x1}=E_{o1}+E_{ac}\exp(j\omega t-j\beta_x x)$ exists within the top 2DEG channel in Fig. 1. We also define the corresponding electron density and velocity as $n_1=n_{o1}+n_{ac}\exp(j\omega t-j\beta_x x)$ and $v_1=v_{o1}+v_{ac}\exp(j\omega t-j\beta_x x)$, respectively. E_{ac}, n_{ac}, and v_{ac} are the amplitudes of the AC electric-field, electron density, and associated velocity, respectively. Here, $\omega(=2\pi f)$ is the angular frequency, and β_x is the propagation constant along the channel (x-direction).

Using (1) and (2), and noting that $J_{ac}=-qv_{o1}n_{ac}-qn_{o1}v_{ac}$, we have

$$J_{ac}=\frac{q^2E_{ac}}{m_e}\frac{j\omega n_{o1}}{\left(j\omega-j\beta_xv_{o1}+\frac{1}{\tau}\right)(j\omega-j\beta_xv_{o1})}. \tag{3}$$

J_{ac} is associated with the channel conductivity σ_{ac1} via $J_{ac}=\sigma_{ac1}E_{ac}$. Thus, we have

$$\sigma_{ac1}=\frac{q^2}{m_e}\frac{j\omega n_{o1}}{\left(j\omega-j\beta_xv_{o1}+\frac{1}{\tau}\right)(j\omega-j\beta_xv_{o1})}. \tag{4}$$

This AC conductivity is the same as that derived previously.[12,21] Using similar steps as above, we can also write the AC conductivity of the lower 2DEG layer in Fig. 1, as

$$\sigma_{ac2}=\frac{q^2}{m_e}\frac{j\omega n_{o2}}{\left(j\omega-j\beta_xv_{o2}+\frac{1}{\tau}\right)(j\omega-j\beta_xv_{o2})}. \tag{5}$$

Having obtained the conductivity of the two channels, we proceed to find the coupled field profiles in the presence of the two channels. Considering the need to enforce field continuity between the two 2DEG channels, we introduce the field components[26,27]

$$E_x=\frac{-1}{\epsilon}\frac{\partial F_z}{\partial y}\quad\text{and}\quad H_z=\frac{-j}{\omega\mu\epsilon}\beta^2F_z, \tag{6}$$

where the potential F_z is given by

$$F_z=\begin{cases}A\cos(\beta_y y)\exp(j\omega t-j\beta_x x) & -d_1\le y\le 0\\ [B\exp(-j\beta_y y)+C\exp(j\beta_y y)]\exp(j\omega t-j\beta_x x) & -d_2<y<-d_1\\ D\exp(\alpha_y y)\exp(j\omega t-j\beta_x x) & y<-d_2.\end{cases} \tag{7}$$

As usual, β_y is the propagation constant in the y-direction for the region $-d_2<y\le 0$ and α_y is the attenuation constant for the region $y\le -d_2$.

Next, we use (7) in the wave equation $\nabla^2F_z+\beta^2F_z=0$ to obtain the dispersion relation $\beta_y^2+\beta_x^2=\beta^2$ and $-\alpha_y^2+\beta_x^2=\beta^2$, where $\beta=\omega\sqrt{\epsilon\mu_o}$ is the propagation constant in the dielectric. Further, $\epsilon=\epsilon_r\epsilon_o$, with ϵ_r being the dielectric constant, ϵ_o is the permittivity, and μ_o is the permeability in vacuum.

In (7), A, B, C, and D are constants to be eliminated by enforcing the boundary conditions at $y=0$, $y=-d_1$, and $y=-d_2$. Prior to applying the boundary conditions, we expand (6) to read

$$E_x=\begin{cases}\frac{A\beta_y}{\epsilon}\sin(\beta_y y)\exp(j\omega t-j\beta_x x) & -d_1\le y\le 0\\ \frac{-j\beta_y}{\epsilon}\left[-B\exp(-j\beta_y y)+C\exp(j\beta_y y)\right]\times\exp(j\omega t-j\beta_x x) & -d_2<y<-d_1\\ \frac{-D\alpha_y}{\epsilon}\exp(\alpha_y y)\exp(j\omega t-j\beta_x x) & y<-d_2,\end{cases} \tag{8}$$

and

$$H_z=\begin{cases}\frac{-j}{\omega\mu\epsilon}\beta^2A\cos(\beta_y y)\exp(j\omega t-j\beta_x x) & -d_1\le y\le 0\\ \frac{-j}{\omega\mu\epsilon}\beta^2\left[B\cos(-j\beta_y y)+C\cos(-j\beta_y y)\right]\times\exp(j\omega t-j\beta_x x) & -d_2\le y\le d_1\\ \frac{-j}{\omega\mu\epsilon}\beta^2D\exp(\alpha_y y)\exp(j\omega t-j\beta_x x) & y<-d_2.\end{cases} \tag{9}$$

To find A, B, C, and D, we enforce the boundary conditions on the tangential E and H-fields across the two 2DEGs. From E-field continuity conditions: $E_x|_{y=-d_1^+} = E_x|_{y=-d_1^-}$ and $E_x|_{y=-d_2^+} = E_x|_{y=-d_2^-}$, we get

$$A\sin(\beta_y d_1) = C\exp(-j\beta_y d_1) - B\exp(j\beta_y d_1), \tag{10}$$

and

$$D\alpha_y \exp(-\alpha_y d_2) = j\beta_y[C\exp(-j\beta_y d_2) - B\exp(j\beta_y d_2)]. \tag{11}$$

Further, from $H_z|_{y=-d_1^+} - H_z|_{y=-d_1^-} = \sigma_{ac1}E_x|_{y=-d_1}$, we have

$$A\left[\frac{j\beta^2}{\omega\mu}\cos(\beta_y d_1) - \sigma_{ac1}\beta_y \sin(\beta_y d_1)\right] = \frac{j\beta^2}{\omega\mu}B\exp(j\beta_y d_1) + \frac{j\beta^2}{\omega\mu}C\exp(-j\beta_y d_1). \tag{12}$$

Likewise, at $y = -d_2$, we have $H_{z(2)}|_{y=-d_2^+} - H_{z(3)}|_{y=-d_2^-} = \sigma_{ac2}E_x|_{y=-d_2}$, giving

$$D\left[\frac{j\beta^2}{\omega\mu}\exp(-\alpha_y d_2) - \sigma_{ac2}\alpha_y \exp(-\alpha_y d_2)\right] = \frac{j\beta^2}{\omega\mu}\left[B\exp(j\beta_y d_2) + C\exp(-j\beta_y d_2)\right]. \tag{13}$$

We can further manipulate (10)–(13), to eliminate all constants A, B, C, and D. This process gives us

$$\frac{\frac{\sigma_{ac1}\beta_y}{\omega\epsilon} - j\cot(\beta_y d_1) - 1}{\frac{\sigma_{ac1}\beta_y}{\omega\epsilon} - j\cot(\beta_y d_1) + 1} = \exp(2j\beta_y \Delta d)\frac{1 + \frac{j\beta_y}{\alpha_y} + \frac{\sigma_{ac2}\beta_y}{\omega\epsilon}}{-1 + \frac{j\beta_y}{\alpha_y} + \frac{\sigma_{ac2}\beta_y}{\omega\epsilon}}, \tag{14}$$

where $\Delta d = d_2 - d_1$. In the above, σ_{ac1} and σ_{ac2} are functions of β_x as described by (4) and (5). Further, β_y and α_y can be written in terms of β_x using the characteristic equation $\beta_x^2 + \beta_y^2 = \beta^2$, with $\alpha_y = \pm j\beta_y$. That is, for a specified frequency, (14) defines the variable β_x. In effect, it represents the dispersion relation of the propagating plasma-wave modes along the x direction in a double channel system. This dispersion relation can be solved numerically using functions like *fzero* or *newtzero* in MATLAB.

We remark that (14) reduces to the known dispersion relation for a single channel system, when $n_{02} = 0$ (leading to $\sigma_{ac2} = 0$). Indeed, setting $\sigma_{ac2} = 0$ in (14), we obtain

$$\frac{\sigma_{ac1}\beta_y}{\omega\epsilon} - j\cot(\beta_y d_1) \pm 1 = 0. \tag{15}$$

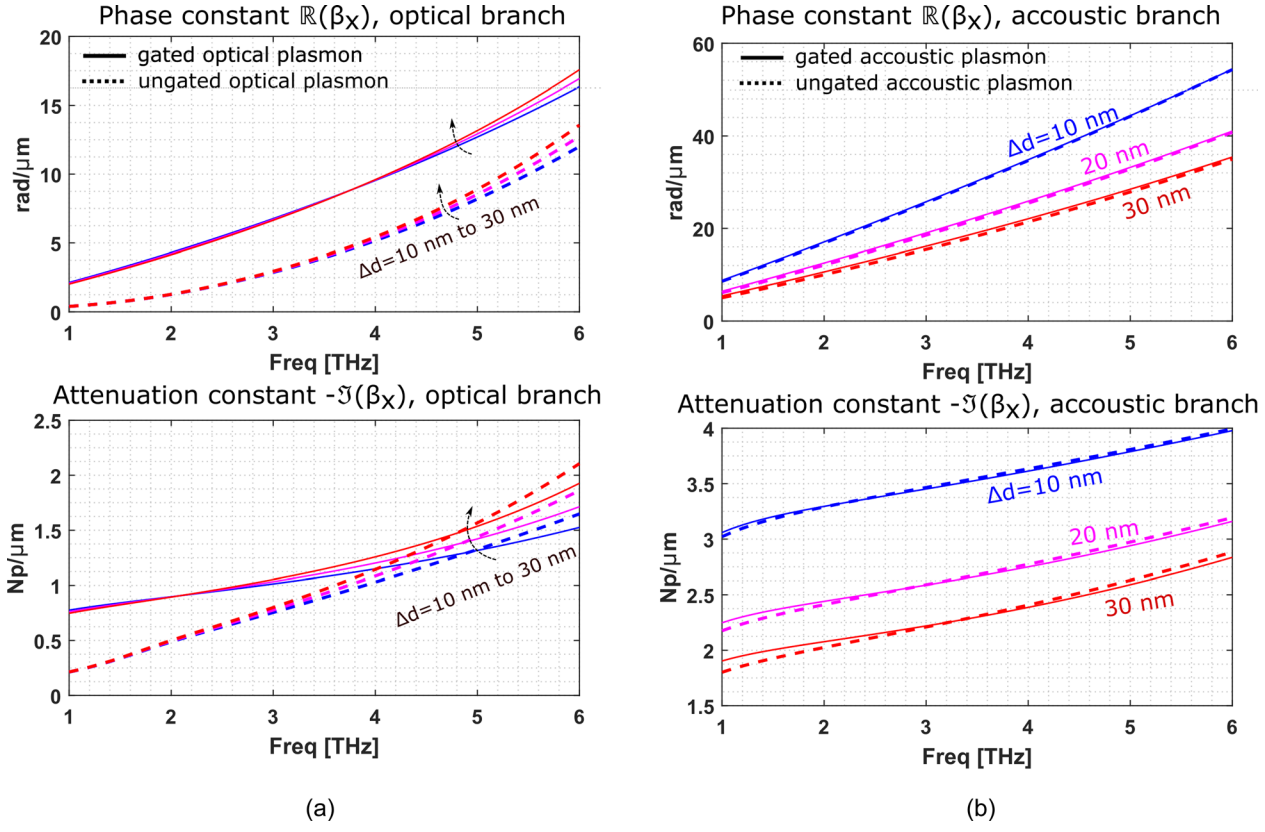

FIG. 2. Dispersion relations for the gated bilayer obtained from (14). The curves correspond to varying inter-channel distance with a fixed $d_1 = 40$ nm. The curves show that the acoustic plasmons are similar to those in the ungated bilayer case. However, the optical plasmons have smaller propagation and higher attenuation constants.

This result is in agreement with the previously derived dispersion relation[12] and serves to verify our calculations.

We note that (14) has four roots signifying two propagating modes in the forward and backward directions. But the two directions are equivalent since we have considered zero drift velocity in the channel. Thus, we need to only plot the solutions for the forward direction. For these plots, we have used the GaN/AlGaN material system with parameters chosen as $n_{o1} = n_{o2} = 7.5 \times 10^{12}\,\mathrm{cm}^{-2}$, $\epsilon_r = 9.5$, $m_e = 0.2m_o$, and the channel mobility $\mu = 1800\,\mathrm{cm}^2/\mathrm{V\,s}$ ($\tau = 0.2$ ps) for both the channels. The obtained modes, referred to as optical and acoustic modes, are shown in Fig. 2. As shown in the figure, the analysis is done for varying Δd with fixed d_1 (=40 nm). We observe that the acoustic modes become increasingly lossy as Δd decreases, whereas the optical modes experience little change. This observation is similar to those for the ungated bilayers. This suggests that the inter-channel distances play the same role in the gated bilayer as in the ungated one.

A comparison with the ungated bilayers ($d_1 \to \infty$ in (14)) reveals that the phase and attenuation constants of the acoustic branch remains unchanged, even for small Δd values. This is because the electric field carried by this mode is confined within the bilayer. Therefore, it does not interact with the gate. However, the optical plasmons interact strongly with the added gate metal. Thus, they have decreased phase velocities and higher attenuation per μm. In conclusion, the gate metal selectively modifies the optical plasmonic modes in the bilayer, while maintaining the acoustic modes as such.

Next, we validate the theoretical calculations using our full-wave-hydrodynamic numerical solver. This solver will also be used to provide more insights on mechanisms of excitation of these modes in the bilayer.

III. STUDY OF EXCITATION OF MODES USING FULL-WAVE HYDRODYNAMIC SOLVER

We first briefly describe the full-wave solver. The developed 2D solver uses a finite difference time domain (FDTD) algorithm to solve Maxwell's and hydrodynamic equations in one or more channels. This hybrid approach provides a self consistent modeling of the electron plasma-fluctuations and the associated fields in the media. A complete description of the solver is provided in Refs. 28–30 and will not be considered here.

We consider a GaN/AlGaN bilayer channel of length 10 μm covered with a metal-gate. To enable excitation from an incident plane wave, we introduce a small gap of length 200 nm in the gate, as shown in Fig. 3. The parameters chosen for this simulation are same as those in Sec. II, except that $d_1 = 28$ nm and $\Delta d = 20$ nm. A broadband terahertz Gaussian pulse is incident on the device and is allowed to couple to the bilayer. The data of the propagating pulse are

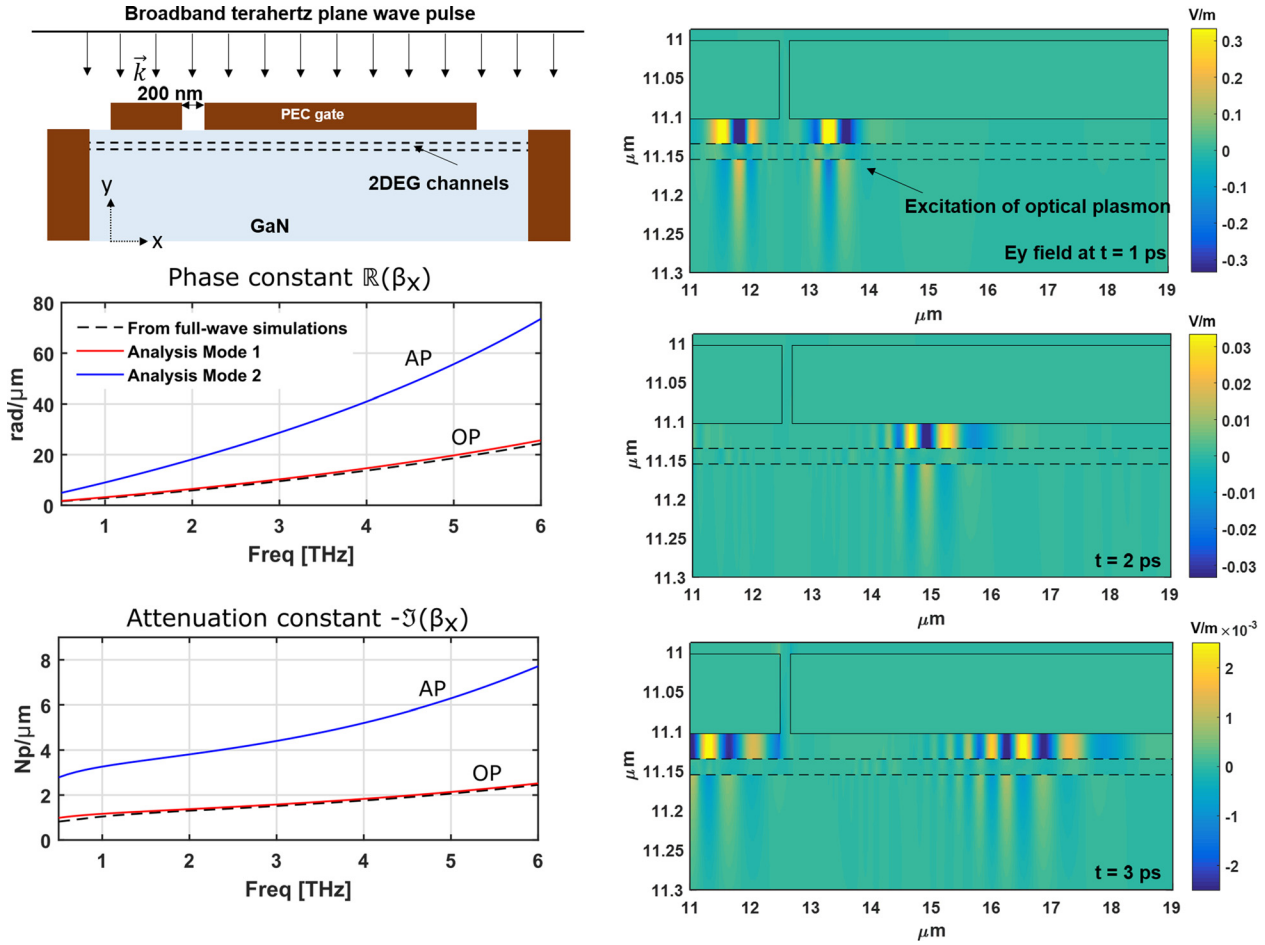

FIG. 3. Schematic of the device used for simulations and corresponding dispersion plots and field plots. AP: acoustic plasmon; OP: optical plasmon.

recorded over time, and subsequently, Fourier transform is calculated to extract the phase and attenuation constants across a band of frequencies. To better understand the plasmon coupling and propagation, we plot the field distribution within and around the channels. Specifically, we plot the E_y (vertical) component to distinctly identify the optical and acoustic modes. As is known, the optical mode is characterized by large E_y field component outside the bilayer, whereas the acoustic mode is mostly confined within the bilayer (channel-pair).

The obtained simulation results are plotted in Fig. 3. We observe that the full-wave simulation results for the phase and attenuation constants are in agreement with the analytical results. Specifically, the simulation results coincide with the optical branch, meaning that the optical modes are excited predominantly. Fig. 3 also includes the time snapshots of the E_y fields at $t = 1$ ps, 2 ps, and 3 ps. The field plots confirm that the incident energy couples primarily to the optical modes in the bilayer. This is evident from small E_y fields between the channels. It is well known that spectra in such experiments are dominated by the optical modes, but this simulation provides further insights. It reveals that the reason for weak acoustic oscillations is its *weaker excitation* rather than stronger attenuation. In other words, the gate discontinuity naturally favors the excitation of the optical modes. This can be reasoned by the fact that ambient incident fields are outside the bilayer—a field profile that matches better with the optical mode field profile. Acoustic modes are difficult to excite due to their confined field-profile that exists between the channels.

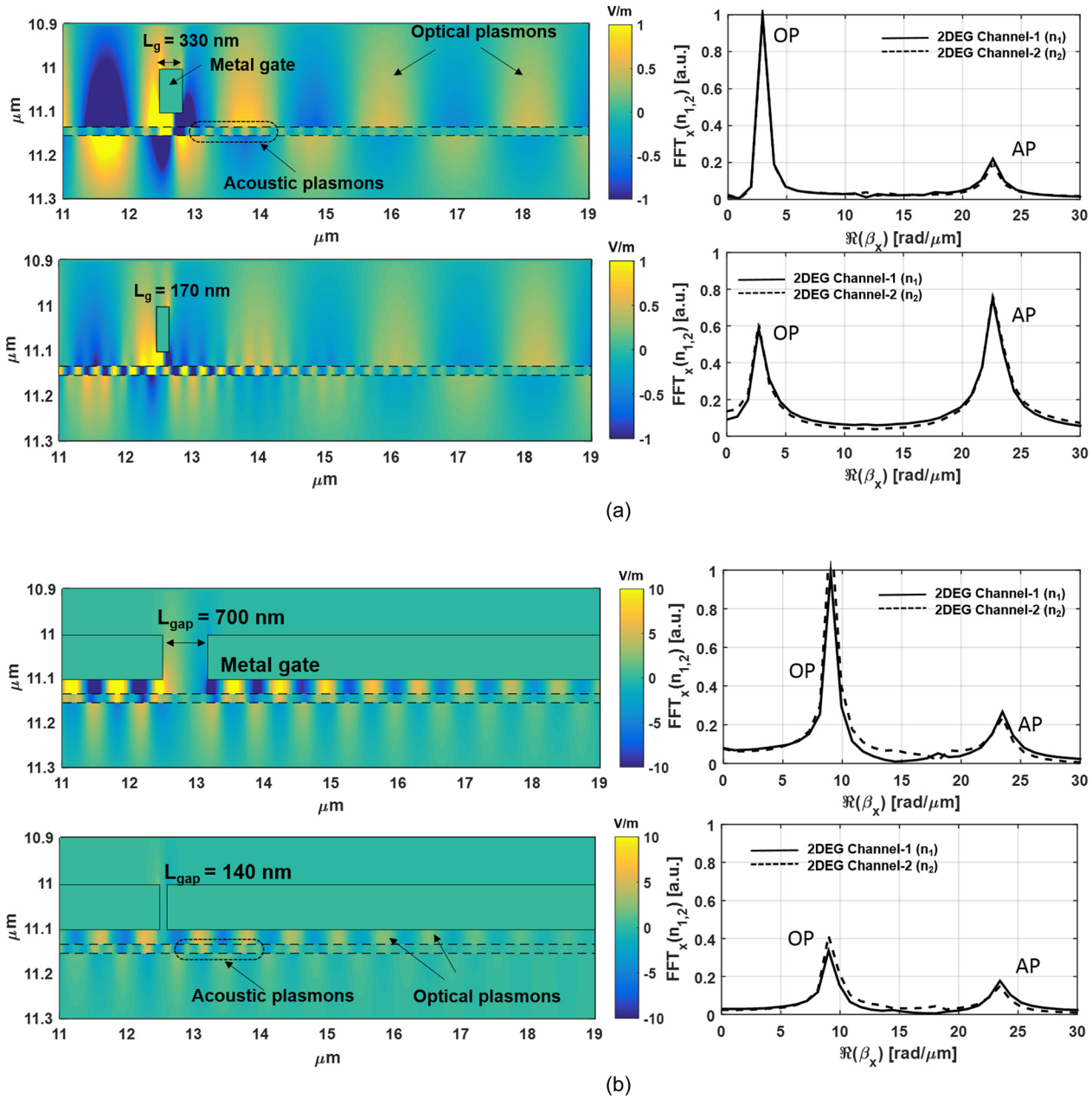

FIG. 4. Excitation and propagation of optical/acoustic modes in the gated/ungated bilayer. (a) Fields in an ungated bilayer with a gap discontinuity. (b) Fields in a gated bilayer with a gate discontinuity. We observe that the spectral content of the oscillations can be controlled by choosing the appropriate gate or gap dimensions. Parameters used: $n_{o1} = n_{o2} = 5 \times 10^{12}$ cm^{-2}, $\mu = 10\,000$ cm^2/V s, $d_1 = 28$ nm, and $\Delta d = 20$ nm.

In summary, we find that numerical and analytical models are in good agreement. We also verify that the optical modes are predominantly excited in a gated-bilayer with a gap discontinuity. We also note that in spite of the tendency for the incident fields to couple to the optical modes, it is possible to selectively excite one mode over another by modifying the gate-gap. Specifically, the gate-gap (or other forms of discontinuity) can be tailored to excite a particular mode. We consider more simulations to test this premise.

First, we consider an ungated bilayer with a small gate that acts as a discontinuity (Fig. 4(a)). We use an incident plane wave as the excitation, but the frequency is chosen to be 3 THz. It is known from the prior simulations that opposite field profiles exist at the two ends of the discontinuity. That is, the discontinuity region acts as a half wavelength cavity. Note that this wavelength can be calculated using (14). Therefore, we consider two cases: (1) when the gate length is $L_g = 330$ nm which is $\lambda_p/2$ for the optical mode and (2) with $L_g = 170$ nm, that is, $\lambda_p/2$ for the acoustic mode. We plot the time snapshots for the field profiles at $t = 12.5$ ps (>steady state time) in Fig. 4(a). On the right, we also show the spectral content of the fluctuations as obtained by spatial Fourier transform of the electron density.

In case-1 ($L_g = 330$ nm), we observe almost 4 times larger wave amplitude for the optical modes as compared with that for the acoustic modes. This strong optical mode excitation comes from the optical mode resonance under the gate. The said resonance mechanism is confirmed from the field plots, where we observe a large E_y field present *outside* the bilayer. This generates an optical-mode field profile. On the contrary, in the second case ($L_g = 170$ nm), a strong E_y field appears between the channels. As expected, this is due to the acoustic mode resonance at the gate. This leads to increased acoustic content in the channels. In conclusion, by setting the gate to a resonant dimension, corresponding spectral content can be enhanced in the channel.

Next, a similar study is conducted for the gated-bilayer. Here, the gate discontinuity size (L_{gap}) was modified. The results (shown in Fig. 4(b)) show similar trends. That is, we observe that the ratio of power in these modes can be controlled by L_{gap}, although we note that total coupled power decreases for the smaller L_{gap} case. This is due to the overall decrease in the exposure of the bilayer to the ambient incident field.

IV. COMPARISON OF SINGLE AND DOUBLE CHANNEL SYSTEMS FOR TERAHERTZ DEVICES

In this section, we compare the dispersion properties of the gated bilayer with that of the corresponding gated single layer. Specifically, we examine the potential of these devices as terahertz detectors. To that end, we consider a case of single and double channel gated HEMTs with parameters as chosen and shown in Table I.

The calculated dispersion curves using (14) and (15), for single and double channels, respectively, are plotted in Fig. 5. Due to ease of excitation and smaller attenuation, an optical branch of the bilayer would be useful for practical applications. Therefore, we show only this branch in Fig. 5.

TABLE I. 2DEG parameters used for the comparison of plasma-wave properties in the gated single and double channel HEMTs. The results are shown in Fig. 5.

	n_{01} (cm^{-2})	n_{02} (cm^{-2})	d1 (nm)	d2 (nm)
Single channel	7.5×10^{12}	…	37	…
Double channel	7.5×10^{12}	7.5×10^{12}	25	50

It is clear that plasma-waves can propagate to longer distances when a double channel HEMT is used. This property is due to the increased electron density supported by the channel-pair. This could be important for the plasma-wave devices based on non-resonant plasma-wave propagation within the channel. More details on the resonant and non-resonant plasma mechanisms for the plasma-wave devices can be found in Refs. 31 and 32.

In addition to the above, the double channel HEMTs are associated with smaller propagation constants. Such increased wavelengths would lead to longer channel lengths for the resonant plasma-wave devices operating at the same frequency. However, we must ascertain that losses per wavelength remain the same as the channel length scales. Therefore, we also calculate this parameter for the single and double channel HEMTs (Fig. 5). We find that the double channel and the single channel HEMTs show about the same loss performance. In conclusion, the advantage lies in the

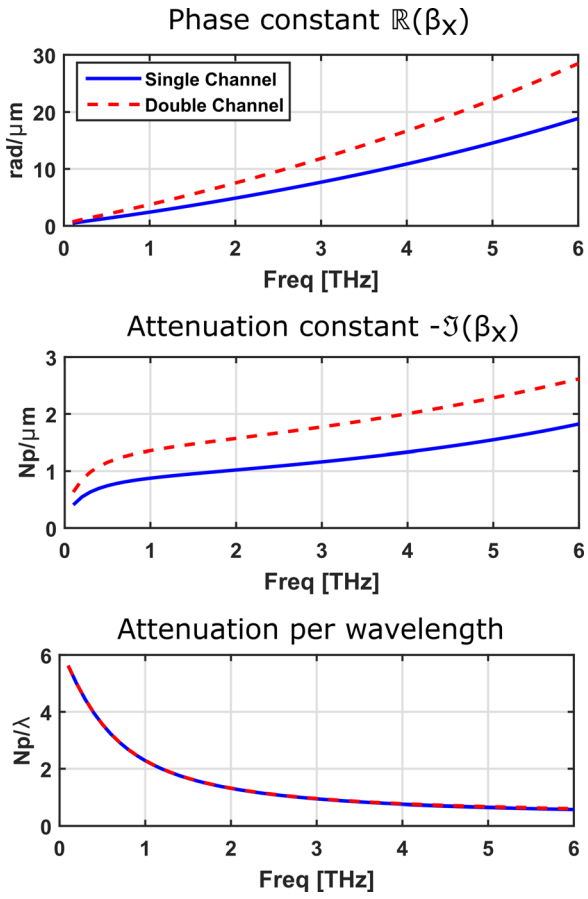

FIG. 5. Comparison of the propagation constant and attenuation constants in the single and double channel HEMTs. The parameters used are defined in Table I.

increased channel dimensions offered by the double channel HEMTs. This leads to larger gate-lengths for the same operational frequency, thus allowing for improved fabrications. Alternatively, we can also say, that the performance can be scaled to larger frequencies when using double channel HEMTs with small gate lengths.

As an example, let us consider a resonant plasma-wave detector at 2 THz. Using the parameters in Table I and assuming channel to be completely covered by a conducting gate, we estimate that the needed channel length would be 315 nm ($\approx\lambda_p/4$) using the double channel HEMT, as opposed to 200 nm using a single channel HEMT. Alternatively, a double channel design with 200 nm channel length would have a resonance at 3 THz. Thus, large gate-length designs and/or higher operational frequencies are possible using the proposed concept.

V. CONCLUSION

We presented dispersion curves and closed form propagation constant formulae for the gated bilayers which could be used for the design of terahertz detectors. The formulae are also verified using physical 2D simulations using the full-wave hydrodynamic numerical model. Our analysis showed that when compared to the ungated bilayer, the addition of a gate selectively affects the optical modes by decreasing their wavelengths and increasing the attenuation constants. Meanwhile, the acoustic modes largely remain unchanged. Using simulations, we further examine the excitation of these modes via an incident plane wave. We find that the most incident energy couples to the optical modes in these scenarios. However, acoustic modes can also be excited, given the discontinuity dimensions are tailored accordingly. We note that the double channel systems are of importance for resonant and non-resonant plasma-wave devices. The non-resonant devices can benefit due to smaller plasmonic losses. For the resonant devices, we can have larger channel lengths (and gate-lengths), allowing for easier fabrications with improved performance.

ACKNOWLEDGMENTS

This work was supported by the Office of Naval Research DATE MURI (Devices and Architectures for Terahertz Electronics Multi-university Research Initiative), under Grant No. N00014-11-1-0721.

[1]W. Knap, Y. Deng, S. Rumyantsev, and M. S. Shur, "Resonant detection of subterahertz and terahertz radiation by plasma waves in submicron field-effect transistors," Appl. Phys. Lett. **81**, 4637 (2002).
[2]A. El Fatimy, F. Teppe, N. Dyakonova, W. Knap, D. Seliuta, G. Valušis, A. Shchepetov, Y. Roelens, S. Bollaert, A. Cappy, and S. Rumyantsev, "Resonant and voltage-tunable terahertz detection in InGaAs/InP nanometer transistors," Appl. Phys. Lett. **89**, 131926 (2006).
[3]X. G. Peralta, S. J. Allen, M. C. Wanke, N. E. Harff, J. A. Simmons, M. P. Lilly, J. L. Reno, P. J. Burke, and J. P. Eisenstein, "Terahertz photoconductivity and plasmon modes in double-quantum-well field-effect transistors," Appl. Phys. Lett. **81**, 1627 (2002).
[4]W. Knap, J. Lusakowski, T. Parenty, S. Bollaert, A. Cappy, V. V. Popov, and M. S. Shur, "Terahertz emission by plasma waves in 60 nm gate high electron mobility transistors," Appl. Phys. Lett. **84**, 2331 (2004).
[5]J. Lusakowski, W. Knap, N. Dyakonova, L. Varani, J. Mateos, T. Gonzalez, Y. Roelens, S. Bollaert, A. Cappy, and K. Karpierz, "Voltage tuneable terahertz emission from a ballistic nanometer InGaAs/InAlAs transistor," J. Appl. Phys. **97**, 064307 (2005).
[6]M. Vosseburger, H. Roskos, F. Wolter, C. Waschke, H. Kurz, K. Hirakawa, L. Wilke, and K. Yamanaka, "Emission of THz radiation from optically excited coherent plasmons in a two-dimensional electron gas," in *Summaries of Papers Presented at the Quantum Electronics and Laser Science Conference, 1996 (QELS'96)* (1996), pp. 206–207.
[7]F. Stern, "Polarizability of a two-dimensional electron gas," Phys. Rev. Lett. **18**, 546–548 (1967).
[8]M. Nakayama, "Theory of surface waves coupled to surface carriers," J. Phys. Soc. Jpn. **36**, 393–398 (1974).
[9]A. Eguiluz, T. K. Lee, J. J. Quinn, and K. W. Chiu, "Interface excitations in metal-insulator-semiconductor structures," Phys. Rev. B **11**, 4989–4993 (1975).
[10]L. Zheng, W. L. Schaich, and A. H. MacDonald, "Theory of two-dimensional grating couplers," Phys. Rev. B **41**, 8493–8499 (1990).
[11]S. J. Allen, D. C. Tsui, and R. A. Logan, "Observation of the two-dimensional plasmon in silicon inversion layers," Phys. Rev. Lett. **38**, 980–983 (1977).
[12]M. Ali Khorrami, S. El-Ghazaly, S.-Q. Yu, and H. Naseem, "Terahertz plasmon amplification using two-dimensional electron-gas layers," J. Appl. Phys. **111**, 094501 (2012).
[13]T. Palacios, A. Chini, D. Buttari, S. Heikman, A. Chakraborty, S. Keller, S. P. DenBaars, and U. K. Mishra, "Use of double-channel heterostructures to improve the access resistance and linearity in GaN-based HEMTs," IEEE Trans. Electron Devices **53**, 562–565 (2006).
[14]S. Heikman, S. Keller, D. S. Green, S. P. DenBaars, and U. K. Mishra, "High conductivity modulation doped AlGaN/GaN multiple channel heterostructures," J. Appl. Phys. **94**, 5321 (2003).
[15]S. D. Sarma and A. Madhukar, "Collective modes of spatially separated, two-component, two-dimensional plasma in solids," Phys. Rev. B **23**, 805 (1981).
[16]R. Z. Vitlina and A. V. Chaplik, "Plasma oscillations of multicomponent two dimensional systems," Sov. Phys. JETP **54**, 536–541 (1981).
[17]D. Kainth, D. Richards, A. Bhatti, H. Hughes, M. Simmons, E. Linfield, and D. Ritchie, "Angle-resolved Raman spectroscopy of the collective modes in an electron bilayer," Phys. Rev. B **59**, 2095 (1999).
[18]S. D. Sarma and E. Hwang, "Plasmons in coupled bilayer structures," Phys. Rev. Lett. **81**, 4216 (1998).
[19]S. Holland, C.-M. Hu, C. Heyn, and D. Heitmann, "Plasmons in tunneling coupled bilayer systems with tunable space symmetry studied by far-infrared spectroscopy," Phys. Rev. B **66**, 073305 (2002).
[20]V. Popov, O. Polischuk, T. Teperik, X. Peralta, S. Allen, N. Horing, and M. Wanke, "Absorption of terahertz radiation by plasmon modes in a grid-gated double-quantum-well field-effect transistor," J. Appl. Phys. **94**, 3556–3562 (2003).
[21]R. Tyson, R. Stuart, H. Hughes, J. Frost, D. Ritchie, G. Jones, and C. Shearwood, "Non-linear Doppler shift of the plasmon resonance in a grating-coupled drifting 2DEG," Int. J. Infrared Millimeter Waves **14**, 1237–1249 (1993).
[22]V. Popov, G. Tsymbalov, and N. Horing, "Tunable anticrossing of gated and ungated plasma resonances and enhancement of interlayer terahertz electric field in an asymmetric bilayer of density-modulated two-dimensional electron gases," Solid State Commun. **140**, 529–532 (2006).
[23]R. S. Howell, E. J. Stewart, R. Freitag, J. Parke, B. Nechay, H. Cramer, M. King, S. Gupta, J. Hartman, P. Borodulin *et al.*, "Low loss, high performance 1-18 GHz SPDT based on the novel super-lattice castellated field effect transistor (SLCFET)," in *2014 IEEE Compound Semiconductor Integrated Circuit Symposium (CSICs)* (IEEE, 2014), pp. 1–5.
[24]M. V. Fischetti, "Depression of the normal-superfluid transition temperature in gated bilayer graphene," J. Appl. Phys. **115**, 163711 (2014).
[25]F. Rana, "Graphene terahertz plasmon oscillators," IEEE Trans. Nanotechnol. **7**, 91–99 (2008).
[26]R. Harrington, *Time-Harmonic Electromagnetic Fields* (Wiley-IEEE Press, 2001).
[27]C. A. Balanis, *Advanced Engineering Electromagnetics*, 2nd ed. (John Wiley and Sons, Hoboken, New Jersey, 2005).
[28]S. Bhardwaj, B. Sensale-Rodriguez, H. G. Xing, S. Rajan, and J. L. Volakis, "Resonant tunneling assisted propagation and amplification of plasmons in HEMTs," J. Appl. Phys. **119**, 013102 (2015).
[29]S. Bhardwaj, N. K. Nahar, S. Rajan, and J. L. Volakis, "Numerical analysis of terahertz emissions from an ungated HEMT using full-wave hydrodynamic model," IEEE Trans. Electron Devices **63**, 990–996 (2016).

[30]M. Khorrami, S. El-Ghazaly, H. Naseem, and S.-Q. Yu, "Global modeling of active terahertz plasmonic devices," IEEE Trans. Terahertz Sci. Technol. **4**, 101–109 (2014).
[31]M. Dyakonov and M. Shur, "Detection, mixing, and frequency multiplication of terahertz radiation by two-dimensional electronic fluid," IEEE Trans. Electron Devices **43**, 380–387 (1996).
[32]W. Knap, M. Dyakonov, D. Coquillat, F. Teppe, N. Dyakonova, J. Łusakowski, K. Karpierz, M. Sakowicz, G. Valusis, D. Seliuta, I. Kasalynas, A. El Fatimy, Y. Meziani, and T. Otsuji, "Field effect transistors for terahertz detection: Physics and first imaging applications," J. Infrared, Millimeter, Terahertz Waves **30**, 1319–1337 (2009).